

# Preparing for Potential Closure of European Airspaces due to Re-entering Space Objects

Enrico Spinielli<sup>✉</sup>, Rainer Koelle<sup>✉</sup> and Quinten Goens<sup>✉</sup>

**Abstract**—The risk of collision between uncontrolled re-entering space debris and aircraft is increasing due to both ever-growing number of airborne flights and of orbiting bodies (and relevant re-entries). National and international authorities need to balance safety and economic impact of adopted measures should a re-entry event be announced, usually on short notice. We employ hourly and daily spatial flight densities calculated from trajectories as recorded by EUROCONTROL’s Network Manager and binned with the Uber H3 geospatial indexing system.

Impact risk probabilities are then calculated based on previous theoretical work. This work enhances the model by employing using actual flown flight trajectories as a basis for time-varying flight densities rather than relying on proxies such as the population density or ADS-B/Mode S message counts. These densities combined with a buffered area along the eventual path of re-entry, can provide mid-air impact probabilities to authorities as an aid for deciding on safety measures such as airspace closures and/or re-routings.

## I. INTRODUCTION

With forecasts predicting a steadily growing number of flights, see Fig. 1, and the modern race to commercialise space it is clear a re-evaluation of the risks of collision and casualties due to uncontrolled debris re-entries is needed. Overseeing authorities need methodologies and tools to assess which safety measures are the most adequate to minimise potential casualties and economic impact.

Surging number of flights in Europe [1] and in the world, but more importantly under development/deployment mega-constellations of satellites in Low Earth Orbit (LEO), such as already active Starlink and OneWeb or planned ones like Kuiper, Starshield, Xingwang et al. will add thousand of orbiting objects with a short operational life. Some of these will inevitably re-enter the Earth’s atmosphere in an uncontrolled manner, cfr. Table I.

This paper develops a practical and straightforward pipeline to rapidly assess the risk from uncontrolled re-entry of space debris for the European region. Apart from the general risk assessment of potential re-entries, a soon to occur re-entry of debris from a 1972 failed USSR mission to Venus is analysed.

## II. METHOD

We follow the same mathematical approach of [2], [3] but instead of approximating flight density with population density [2] or aircraft transponder data [3], we use actual flown flight trajectories.

The hourly flight density estimation is based on on flown Instrument Flight Rules (IFR) trajectories as recorded by EU-

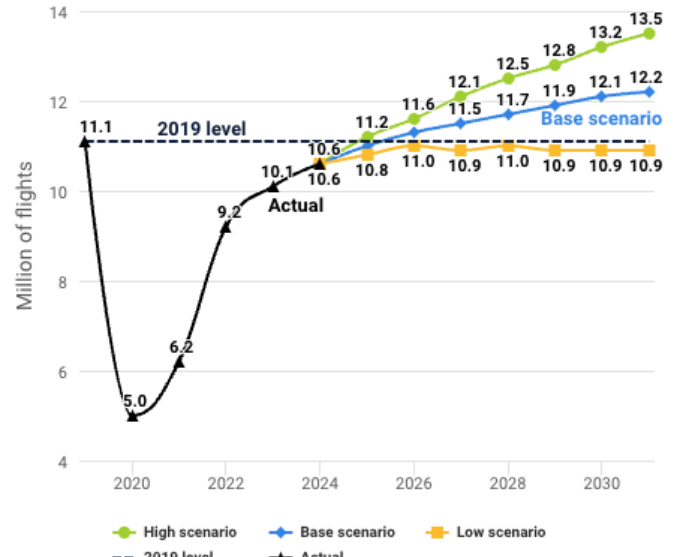


Fig. 1: EUROCONTROL 7-year forecast 2025-2031 (Spring 2025).

Constellation	Country	Launched	Active	Planned	First launch
Starlink	US	4714	3521	4714	2018
Starlink2A	US	3689	3070	6720	2022
Starlink2	US	0	0	30456	-
OneWeb	UK	660	635	716	2019
OneWeb2	UK	0	0	2304	-
Kuiper	US	29	27	3232	2023
StarShield	US	193	126	32	2022
Xingwang	CN	50	10	996	2021
Qianfan	CN	90	28	32	2024
Guangwang	CN	0	0	12992	-
Yinhe	CN	8	7	1000	2020
Hanwha	KR	0	0	2000	-
Lynk	US	10	6	2000	2020
Astra	US	0	0	13620	-
Telesat	CA	0	0	300	-
HVNET	US	0	0	1440	-
SpinLaunch	US	0	0	1190	-
Globalstar3	DE	0	0	3080	-
Honghu-3	CN	0	0	10000	-
Semaphore	FR	0	0	116640	-
E-Space	US	4	0	337323	2022

Table I: Megaconstellations (planned > 1000) as per filing to the International Telecommunication Union (ITU)

ROCONTROL’s Network Manager (NM)<sup>1</sup> and binned using Uber’s H3 geospatial indexing system [4] in order to decrease

<sup>1</sup>NM coordinates Air Traffic Flow and Capacity Management (ATFCM) operations on behalf of EUROCONTROL’s 42 Member States and 2 Comprehensive Member States covering almost all European Civil Aviation Conference (ECAC) States.

spatial complexity which in turn enables fast processing. This work will use H3 cells at resolution 3 which corresponds to hexagons of an average area  $12\,393 \text{ km}^2$  and an average edge length of  $68.979 \text{ km}$  [5] as depicted in Fig. 2.

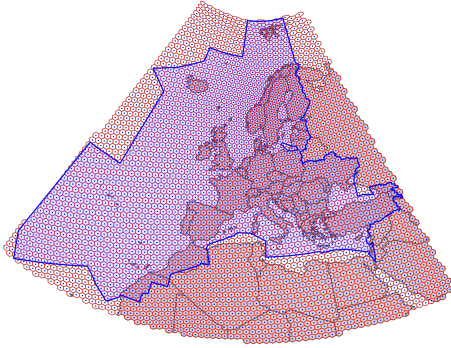


Fig. 2: H3 cells (red) at resolution 3 and their centers (blue) covering the bounding box of 43 EUROCONTROL Member States Flight Information Region (FIR)s (blue shaded polygon).

The flight densities are characterised on an hourly basis for all days in the busiest International Air Transport Association (IATA) summer ISO week in 2023 and 2024.

This paper expands the works of [2], [3] and provides a reproducible example for States, Agencies or relevant authorities to build upon.

Next sections will develop the mathematical background for the evaluation of collision and casualties risk of which traffic density is a key component.

Fig. 3 shows hourly flight density for the 5th of July 2024. Expected outcomes such as cells at zero density for war or no-fly zones (Ukraine, Libia or Syria) or typical traffic flows (North Atlantic, Canaries and East-bound over Türkiye) are clearly highlighted.

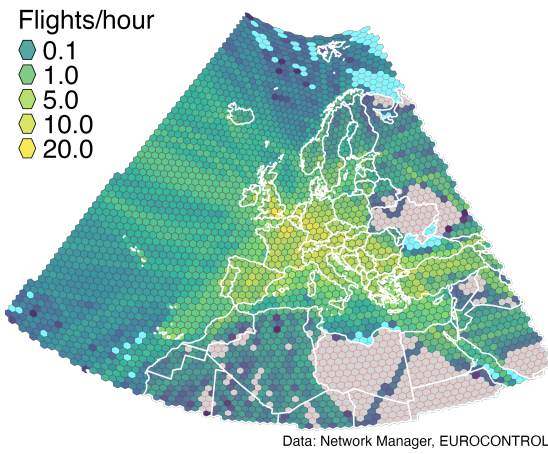


Fig. 3: Flight density in the EUROCONTROL Area on the 5th of July 2024, the busiest day of the busiest week in 2024 (H3 cells at resolution 3).

#### A. Impact probability for a single flight and single debris

The probability,  $p_k$ , of a debris (point) object  $k$ , impacting an aircraft (point) object over the area,  $a$ , is expressed as:

$$p_k = \varepsilon_k \int_a \rho(\vec{x}) \sigma_k(\vec{x}) da$$

where  $\rho(\vec{x})$  is the probability density of an aircraft in  $\vec{x}$ ,  $\sigma(\vec{x})$  is the impact probability density of a debris object  $k$  in the position  $\vec{x}$  and  $\varepsilon_k$  is the effective exposed area, i.e. the effective risk area for the  $k^{th}$  debris object impacting the aircraft (see Section II-B later on).

Using H3 to discretise the area of interest  $a$  using H3 cells gives

$$p_k = \varepsilon_k \sum_h \rho(h) \sigma_k(h).$$

Where for each cell  $h$  the following applies

$$p_k(h) = \varepsilon_k \rho(h) \sigma_k(h).$$

#### B. Aircraft effective exposed area

It is assumed the aircraft impact area to be much larger than the debris object area so as to neglect the debris impact area. The geometry of the aircraft is simplified and modelled as a rectangular cuboid with dimensions of wingspan, length and height. Now, if the aircraft were stationary, the area exposed to a debris impact would be the top view, while if the debris were stationary it would be the front view. In reality an aircraft enroute is moving (mainly) horizontally and the debris vertically <sup>2</sup>, which which allows to express the effective exposed area,  $\varepsilon_k$ , as

$$\varepsilon_k = \frac{s_a a_h + s_{d_k} a_v}{s_{d_k}}$$

where  $s_a$  is the average aircraft speed,  $s_{d_k}$  is the average fall speed of the  $k$ -th debris object,  $a_T$  area of the aircraft as viewed from the top,  $a_F$  area of the aircraft as viewed from the front of the aircraft.

In the calculations the following is assumed to be true ( $t$  subscript for aircraft type)

- constant debris fall speed  $s_{d_k} = 145 \text{ mph} = S$
- constant aircraft speed,  $s_a = C_t$ , equal to its cruise speed,
- aircraft area as viewed from the top,  $a_T = W_t \times L_t = A_t$ , where  $W_t$  is the wingspan, and  $L_t$  the length for the specific aircraft type  $t$
- aircraft area as viewed from the front,  $a_F = W_t \times H_t = F_t$ , where  $W_t$  is the wingspan, and  $H_t$  the height for the specific aircraft type  $t$

The effective exposed area now only depends on the aircraft type  $t$  (dimensions and cruise speed) and can be rewritten as:

$$\varepsilon_t = \frac{C_t F_t + S A_t}{S}$$

The values  $W_t$ ,  $H_t$  and  $L_t$  have been retrieved from [6]–[8].

<sup>2</sup>Even for a ballistic coefficient of  $50 \text{ lbs/ft}^2$ , the flight path angle of a re-entering object at 40,000 feet is -86.6 degrees, which corresponds to nearly vertical descent. Since most debris objects have ballistic coefficients equal to or less than  $50 \text{ lbs/ft}^2$ , the vertical descent assumption is a very accurate approximation. [2]

The impact probability for cell  $h$  and single aircraft of type  $t$  becomes:

$$p_{t,k}(h) = \varepsilon_t \rho_t(h) \sigma_k(h)$$

### C. Impact probability density for debris of inclination $i$

Debris that reenter the Earth's atmosphere via drag-induced decay will fly circular orbits prior to re-entry even if initially on elliptical ones.<sup>3</sup>

The angular position,  $\theta$ , of the re-entry point from the ascending node, see Section VI, is uniformly distributed for uncontrolled reentries,  $\sigma(\theta) = 1/(2\pi)$ . This is due to uncertainties in atmospheric drag and the gravitational effects of the Equatorial bulge. Hence we assume that the impact longitude,  $\lambda$ , is uniformly distributed.

The impact probability density,  $\sigma(\varphi, i)$ , at latitude  $\varphi$  of a reentering object whose orbit has inclination  $i$  (see Fig. 10) is given by [Equation 15 in [2]]:

$$\sigma(\varphi, i) = \frac{1}{2\pi^2 R^2 \sqrt{(\sin^2(i) - \sin^2(\varphi))}} \quad (1)$$

where  $R$  is the distance from the center of the Earth of the object potentially being impacted by the debris.

So for example if a building is located at latitude 30 degrees and has an area of 1000 m<sup>2</sup> and a piece of debris reenters the Earth's atmosphere from an orbit having an inclination of 45 degrees, the impact probability is given by

$$P = \Delta A \times \sigma(\varphi, i) = 1000 \times \sigma\left(\frac{\pi}{6}, \frac{\pi}{4}\right) \\ = 1000 \times 2.490\,756 \times 10^{-15} = 2.490\,756 \times 10^{-12}$$

where we used the equatorial value of 6378 km, for the Earth's radius,  $R$ , as the distance of the building from the center of the planet.

The impact probability density  $\sigma(\varphi, i)$  for an inclination  $i$  of 51.7° is plotted in Fig. 4 and takes a characteristic U shape.

### D. Impact probability density for debris

If we consider historical debris re-entry data, we can numerically derive the debris impact probability as a weighting function by summing up and averaging all single densities:

$$\sigma(\varphi) = \sum_k \sigma(\varphi, i_k)$$

From [9] we extracted 1968 debris re-entries during 25 calendar years from 1st Jan 2000 till 31st Dec 2024. The result of combining all the U-shaped densities can be seen in Fig. 5.

Spatially combining  $\sigma(\lambda, \varphi)$  for the H3 cells in the NM area we obtain the weightings per cell (per hour) as in Fig. 6.

<sup>3</sup>In fact drag at perigee will lower apogee and similarly drag at apogee will lower perigee. But because drag at perigee is higher due to denser atmosphere, the apogee will decrease faster than perigee and the orbit will then tend to be a circular one.

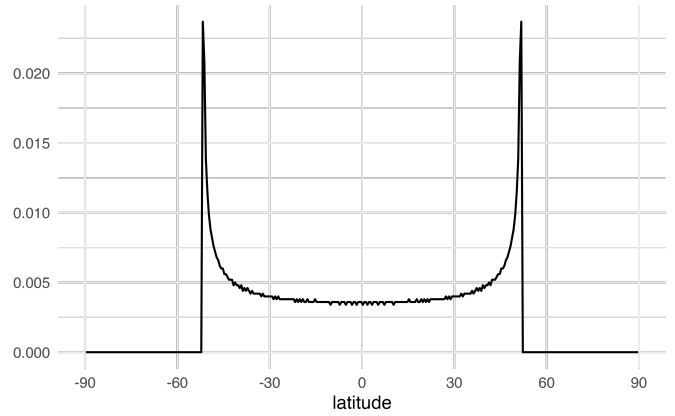


Fig. 4: Impact probability density  $\sigma(\varphi, i = 51.7)$  for debris of inclination  $i$  and altitude 550 km.

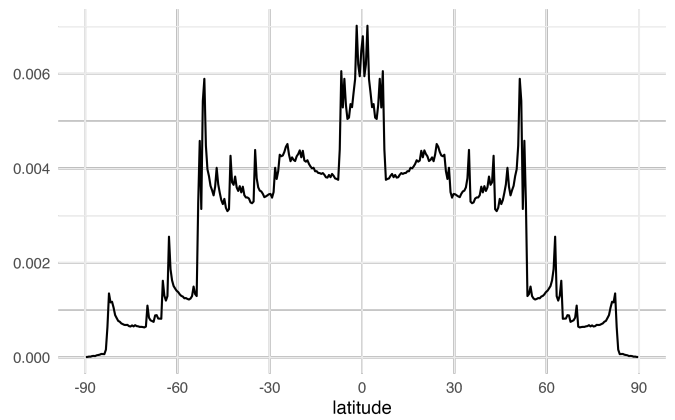


Fig. 5: Weighting function derived from 25 years of re-entries as an empirical approximation of  $\sigma(\varphi)$ .

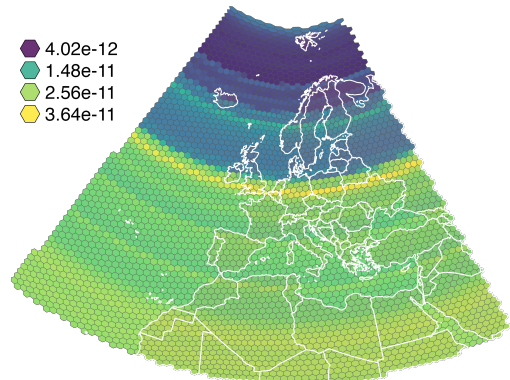


Fig. 6: Weightings for H3 cells in NM area.

### E. Hourly impact probability per H3 cell

By combining the hourly aircraft density (per aircraft type) with the relevant weightings per H3 cell, we can numerically compute the hourly impact probability for each hexagonal cell as:

$$E_h = \sum_t W(h) \cdot \rho_t(h) \cdot \varepsilon_t$$

where  $E_h$  is the collision expectation in the hexagon  $h$ ,  $W(h)$  is the median value of the weighting function over the area of hexagon  $h$ ,  $t$  is the International Civil Aviation Organization (ICAO) aircraft type,  $\rho_t(h)$  is the traffic density for type  $t$  in cell  $h$  and  $\varepsilon_T$  is effective exposed area for aircraft of type  $t$ .

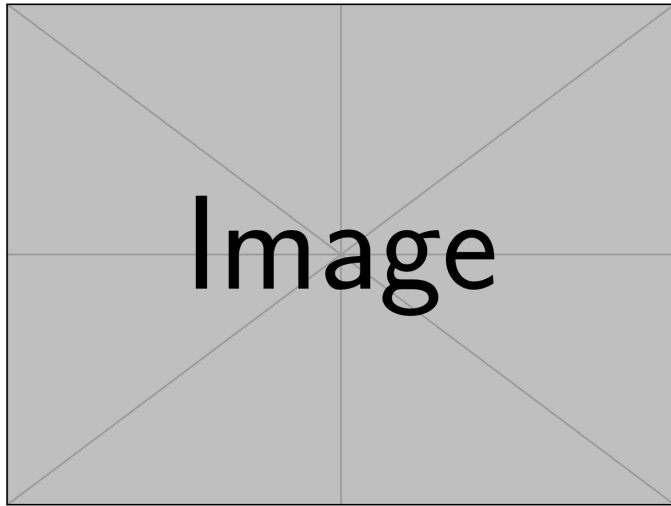


Fig. 7: Collision risk probability.

### F. Use Case: KOSMOS 482 Descent Craft re-entry

In few days (at the time of writing this paper) at 6h May 10, 2025 ( $\pm 2.8$  days), the KOSMOS 482 Descent Craft should reenter the Earth's atmosphere **?**. This is supposedly the lander module from a 1972 failed Soviet Venera mission [10] of 480 kg weight and circa 1 m diameter. Being supposed to survive Venus's atmosphere which is much denser and hotter than Earth's atmosphere (surface pressure 93 times that of Earth and temperatures reaching 467 degrees Celsius (872 degrees Fahrenheit)). So it could re-enter Earth intact and not break into smaller fragments some of which could burn up.

With what developed in this paper, we can derive the casualty risk and determine the maximum value using data for the busiest day in the busiest 2024 week.

Once the re-entry track is known more or less accurately, the relevant H3 cells can be

### III. DATA AND CODE FOR REPRODUCIBILITY

We have calculated collision and casualty risk probabilities for the two busiest weeks in 2023 and 2024. The relevant dataset represents a data cube as logically depicted in

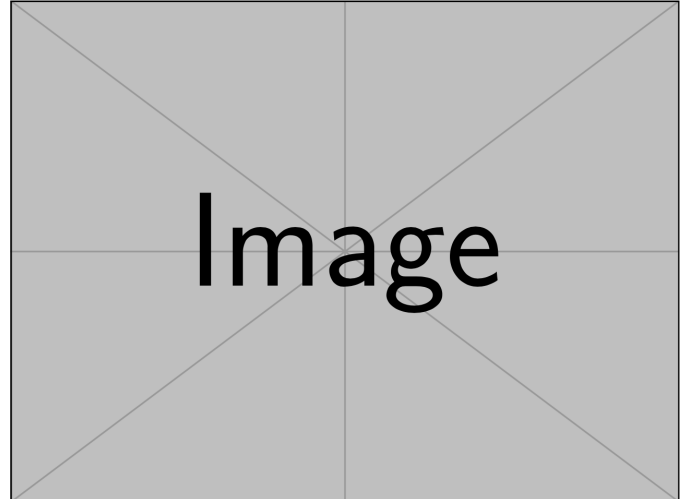


Fig. 8: Casualty for KOSMOS 482 Descent Craft re-entry.

Fig. 9 is available in the companion GitHub repository of the paper at [https://github.com/espinelli/flight\\_density\\_space\\_debris](https://github.com/espinelli/flight_density_space_debris). We have also developed a companion R package aviodebris to heavylift the various data processing steps to produce the results in the paper; it is available at <https://github.com/espinelli/aviodebris>.

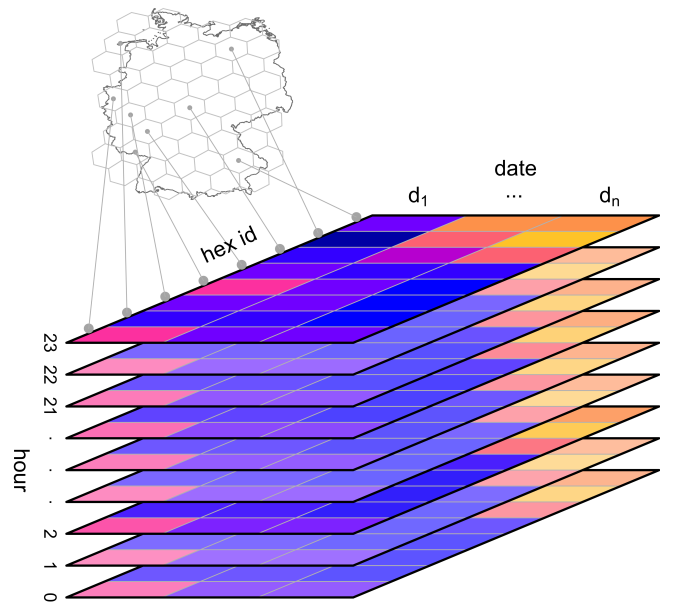


Fig. 9: Data cube of hourly flight densities data over H3 hexes (in Germany as an example) for multiple dates,  $d_1 \dots d_n$ .

### IV. CONCLUSION AND FUTURE WORK

We show how National and/or International authorities could prepare for the more and more likely and frequent occurrence of uncontrolled re-entry of space objects that could pose a safety concern on civilian aviation. The techniques we implemented on realistic data and sound algorithms can contribute to the bag of tools in the hands of technical and

political entities aiming at guaranteeing the utmost safety and minimal economic disruption to civil aviation in Europe.

Future work will explore the impact of megacostellations and the risk for European airspace.

## V. APPENDIX

### VI. ORBITAL ELEMENTS

We refer to Fig. 10 to describe the orbital parameters of interest for the current work.

The angular position,  $\theta$ , of the re-entry point from the ascending node in the orbit plane is  $\theta = \omega + \nu$ . It is related to the latitude,  $\varphi$ , via the Cartesian coordinate  $k$ ,  $k = R \sin(\varphi) = R \sin(\theta) \sin(i)$ , or

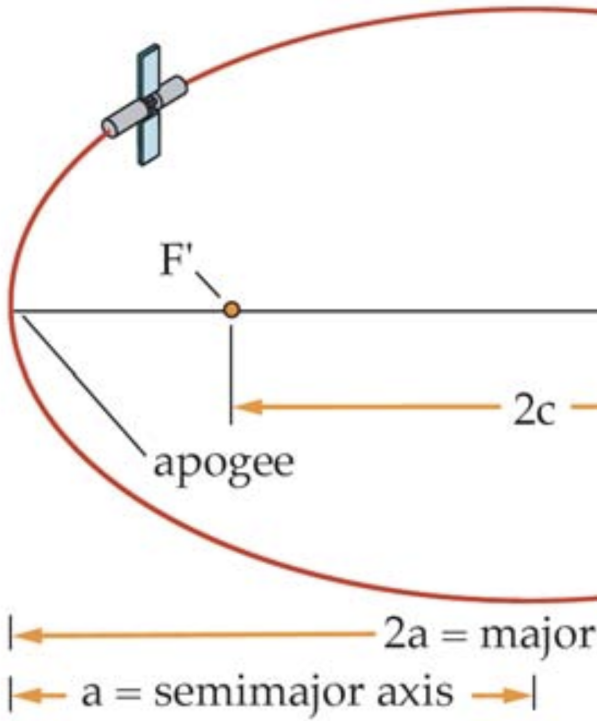
$$\sin(\varphi) = \sin(\theta) \sin(i) \quad (2)$$

Mass of Earth,  $M_{\oplus} = 5.9722 \times 10^{24}$  kg.

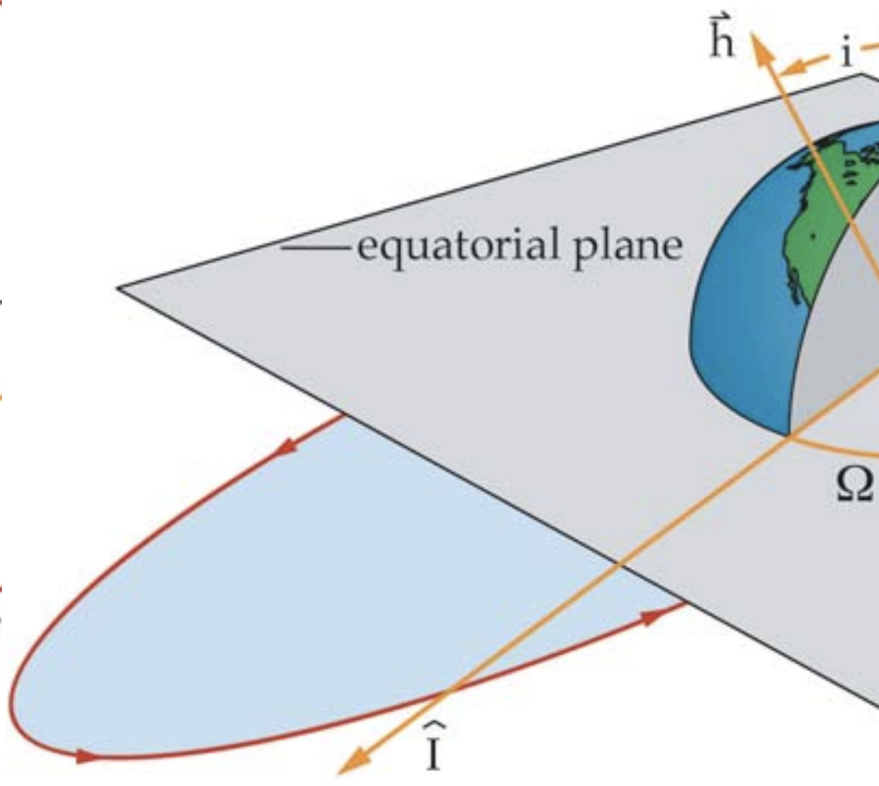
These are used to derive numerically compute the weighting function, Fig. 4: for debris with inclination  $i$  we simulate an orbit of  $N$ , i.e. 10001, positions and calculate the corresponding cartesian position and the equivalent longitude and latitude.

## REFERENCES

- [1] Statfor, “EUROCONTROL Forecast Update 2025-2031 - Spring Update | EUROCONTROL,” 28-Feb-2025. [Online]. Available: <https://www.eurocontrol.int/publication/eurocontrol-forecast-2025-2031>. [Accessed: 29-Apr-2025]
- [2] R. P. Patera, “Hazard Analysis for Uncontrolled Space Vehicle Reentry,” *Journal of Spacecraft and Rockets*, vol. 45, no. 5, pp. 1031–1041, Sep. 2008 [Online]. Available: <https://arc.aiaa.org/doi/10.2514/1.30173>. [Accessed: 23-Mar-2025]
- [3] E. Wright, A. Boley, and M. Byers, “Airspace closures due to reentering space objects,” *Sci Rep*, vol. 15, no. 1, p. 2966, Jan. 2025 [Online]. Available: <https://www.nature.com/articles/s41598-024-84001-2>. [Accessed: 06-Feb-2025]
- [4] Uber Technologies Inc., “H3: Uber’s hexagonal hierarchical spatial index.” [Online]. Available: <https://eng.uber.com/h3>
- [5] “Tables of Cell Statistics Across Resolutions | H3.” [Online]. Available: <https://h3geo.org/docs/core-library/restable>. [Accessed: 07-Feb-2025]
- [6] EUROCONTROL, “Aircraft Performance Database.” [Online]. Available: <https://contentzone.eurocontrol.int/aircraftperformance/>. [Accessed: 29-Jan-2025]
- [7] “SKYbrary Aviation Safety.” [Online]. Available: <https://skybrary.aero/>. [Accessed: 11-Apr-2025]
- [8] “Doc 8643.” [Online]. Available: <http://www.doc8643.com>. [Accessed: 11-Apr-2025]
- [9] J. C. McDowell, “General Catalog of Artificial Space Objects.” 2020 [Online]. Available: <https://planet4589.org/space/gcat>. [Accessed: 02-Mar-2025]
- [10] “The Space Review: Kosmos 482: Questions around a failed Venera lander from 1972 still orbiting Earth (but not for long).” [Online]. Available: <https://www.thespacereview.com/article/4384/1>. [Accessed: 30-Apr-2025]
- [11] J. J. Sellers *et al.*, *Understanding space: An introduction to astronautics*. McGraw-Hill Custom Pub., 2003 [Online]. Available: <https://books.google.be/books?id=IlcgAQAAIAAJ>



(a) Keplerian elements: semi-major axis,  $a$ , the distance between the foci,  $2c$ , the eccentricity,  $e = (2c)/(2a)$ . (the semiparameter (a.k.a. *semilatus rectum*),  $p$ , describes the size of the conic section by defining the width at the primary focus, and is defined as  $p = b^2/a = a(1 - e^2)$ )



(b) Keplerian elements: inclination,  $i$ , the right ascension of the ascending node,  $\Omega$ , and the argument of periaxis,  $\omega$ . (Earth rotates around  $\hat{K}$ )

Fig. 10: Definition of Keplerian elements. The orbital elements describing the trajectory of orbiting object are illustrated in association with an inertial reference frame  $\hat{I}\text{-}\hat{J}\text{-}\hat{K}$ . The  $I$ -axis,  $\hat{I}$ , points toward the vernal equinox and the  $J$ -axis,  $\hat{J}$ , is perpendicular to the  $I$ -axis in the equatorial plane n the sense of Earth's rotation with the  $K$ -axis pointing up. The semi-major axis,  $a$ , the eccentricity,  $e$ , the inclination,  $i$ , the right ascension of the ascending node,  $\Omega$ , and the argument of perigee,  $\omega$ , constitute, together with the mean anomaly at the initial position,  $M_0$ , a set of six constants of motion that are preserved in the absence of perturbation. True anomaly,  $\nu$ , specifies the location of an orbiting object within the orbit. It is the angle between perigee and the orbiting object's position vector measured in the direction of the orbiting object's motion. Figures from [11], respectively Figure 5-2 and Figure 5-9.